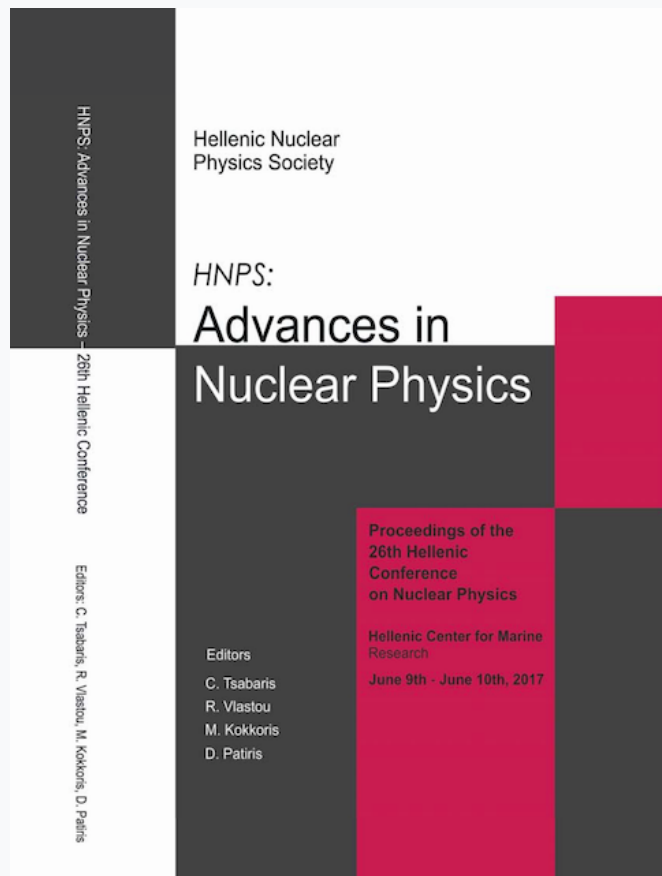


HNPS Advances in Nuclear Physics

Vol 25 (2017)

HNPS2017



Investigation of JET ITER-like wall Be marker tiles

P. Tsavalas, A. Lagoyannis, K. Mergia, K. Triantou, S. Harissopoulos, M. Rubel, P. Petersson, M. Kokkoris, and JET Contributors

doi: [10.12681/hnps.1965](https://doi.org/10.12681/hnps.1965)

To cite this article:

Tsavalas, P., Lagoyannis, A., Mergia, K., Triantou, K., Harissopoulos, S., Rubel, M., Petersson, P., Kokkoris, M., & JET Contributors, and. (2019). Investigation of JET ITER-like wall Be marker tiles. *HNPS Advances in Nuclear Physics*, 25, 141–146. <https://doi.org/10.12681/hnps.1965>

Investigation of JET ITER-Like Wall Be Marker Tiles

P. Tsavalas^{1,4,*}, A. Lagoyannis², K. Mergia¹, K. Triantou¹, S. Harissopoulos²,
M. Rubel³, P. Petersson³, M. Kokkoris⁴ and JET Contributors^{**}

¹*National Centre for Scientific Research “Demokritos” Institute of Nuclear and Radiological Science and Technology, Energy and Safety, 15310 Aghia Paraskevi, Athens, Greece*

²*National Centre for Scientific Research “Demokritos”, Institute of Nuclear and Particle Physics, 15310 Aghia Paraskevi, Athens, Greece*

³*Department of Fusion Plasma Physics, Royal Institute of Technology (KTH), 10044 Stockholm, Sweden*

⁴*National Technical University of Athens, Department of Physics, Zografou Campus, Athens, Greece*

^{**}*See the author list in: X. Litaudon et al., Nuclear Fusion Special issue: 26th Fusion Energy Conference (Kyoto, Japan, October 2016)*

Abstract

The JET tokamak is operated with beryllium and tungsten plasma-facing components to prepare for the exploitation of ITER. Marker tiles were installed in the limiters and divertor in order to determine the erosion and deposition. Specimens from different Be marker tiles of the ITER – Like wall JET tokamak main chamber and from the exposure periods 2011-2012 and 2013-2014 were investigated using nuclear reaction analysis, X-ray fluorescence spectroscopy and scanning electron microscopy in order to assess the deposition focusing on the C deposition, erosion and surface morphology.

Carbon was detected on surface of all the samples, while its surface atomic density and the deposition depth range from $(0.35 \pm 0.07) \times 10^{17}$ to $(11.8 \pm 0.6) \times 10^{17}$ at/cm² and from 0.4 to 6.7 μm , respectively. Tungsten is, also, detected in samples. Finally, partial or strong erosion was observed on the surface of most of the samples, while the morphology of sample surfaces presents significant differences comparing with the reference one.

Keywords beryllium marker tiles, carbon deposition, erosion, NRA, XRF, SEM

1. Introduction

The Joint European Torus (JET) the largest experimental fusion device with plasma magnetic confinement, investigates the potential of fusion power as a future energy source [1]. Its main scientific mission is to develop plasma operation scenarios for a reactor-class machine such as ITER. This includes also the performance test of plasma-facing materials (PFM) and components (PFC).

In 2010/11 the plasma facing material of JET tokamak was changed from carbon to a combination of metallic elements. More specifically, the first wall of the main chamber was covered with Be, while the divertor was covered with W [2,3]. Additionally, marker tiles were posed as erosion – deposition diagnostic tools [3]. The marker tiles of the main chamber consisted of a thin Be top layer (8-10 μm), a Ni interlayer (2-3 μm) and bulk Be [4].

Three experimental campaigns (ILW-1 2011/12, ILW-2 2013/14 and ILW-3 2015/16) with different operational characteristics were carried out. In the current work, samples from different marker tiles of the main chamber and the first 2 campaigns were analyzed to understand the effects of plasma on the surface of the plasma-facing materials using the following analytical techniques: Nuclear Reaction Analysis (NRA), X-ray Fluorescence Spectroscopy (XRF) and Scanning Electron Microscopy (SEM) with Energy Dispersive Analysis (EDS).

* Corresponding author. Tel. +30 2106503770; email: patsavalas@ipta.demokritos.gr

2. Sample and Experimental Details

Fig. 1a shows the poloidal cross section of the JET tokamak and the position of the marker tiles, whereas in Fig. 1b the pictures of the marker tiles and the position of the investigated samples are depicted. Table 1 presents the investigated samples from the various positions of the JET tokamak which are shown in Fig. 1. The nominal composition of the marker tiles before the plasma exposure was Be (bulk)/ Ni ((2.5 ± 0.5) μm)/ Be ((8 ± 1) μm) where the nickel is used as interlayer in order to assess the erosion of the surface. Additionally, a sample with composition Be (bulk)/ Ni ((2.6 ± 0.1) μm)/ Be ((7.6 ± 0.1) μm) was used as reference sample.

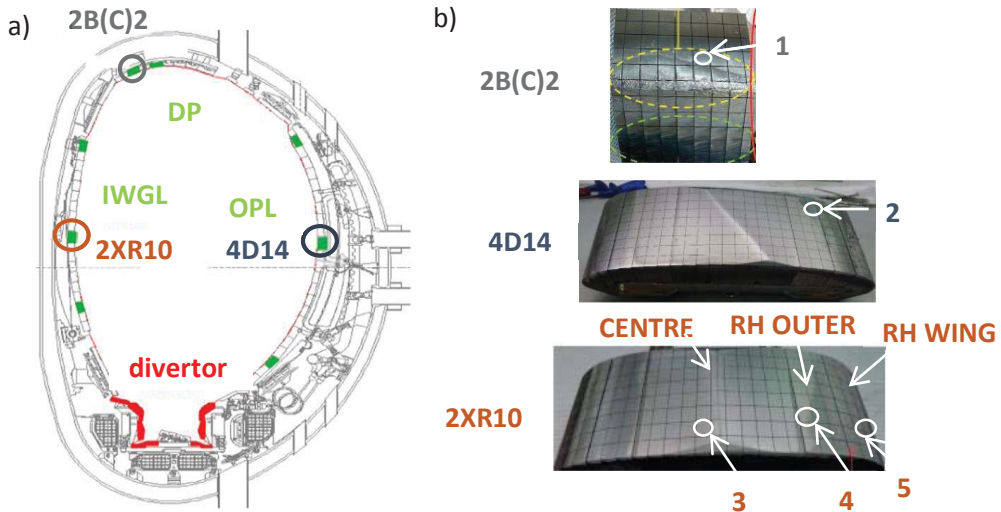


Fig. 1: (a) Poloidal cross section of the JET tokamak and the position of the tiles in the main chamber and (b) pictures of the marker tiles and the position of the samples

The carbon depth profile was determined with the NRA technique using the interaction $^{12}\text{C}(\text{d},\text{p}_0)^{13}\text{C}$ and employing the cross section of [5]. The NRA measurements were carried out at the 5.5 MeV Tandem accelerator of NCSR “Demokritos”. The samples were irradiated with a 1.35 MeV deuterium beam and the products were detected at 170 degrees with respect to the beam axis by a silicon surface barrier detector. A kapton foil, with thickness of 14 μm , was used in order to avoid the overlapping of $^{12}\text{C}(\text{d},\text{p}_0)^{13}\text{C}$ peak with the alpha peaks from Be. The experiment was carried out under high vacuum (10^{-7} mbar). Additionally, for the current research the cross section of the $^9\text{Be}(\text{d},\text{p}_0)^{10}\text{Be}$ reaction was used. The evaluation of the data was performed using the SimNRA program [6].

The XRF measurements were conducted using Amptek’s system with an Ag X-ray tube, a high voltage of 30 kV and a silicon drift detector [7]. A collimator of 1 mm diameter was used. Elements with $Z > 11$ are detected with a detector limit in the order of ppm. Quantification was achieved employing XRF-FP X-ray analysis software and using a NIST stainless steel 316 standard [8]. SEM measurements were carried out on a FEI Quanta Inspect SEM coupled with Energy Dispersive Spectroscopy (EDS). For the EDS a voltage of 12.5 kV was used.

3. Results and Discussion

The $^{12}\text{C}(\text{d},\text{p}_0)^{13}\text{C}$ peak was observed in NRA spectra of all the samples. The presence of the C is due to remnants from the previous wall and migration of other parts of the JET chamber which still consist of C [3]. Fig. 2 shows a representative experimental spectrum of the OPL (120) sample and the simulation of the $^9\text{Be}(\text{d},\text{p}_0)^{10}\text{Be}$ and $^{12}\text{C}(\text{d},\text{p}_0)^{13}\text{C}$ reactions. The cross section of the $^9\text{Be}(\text{d},\text{p}_0)^{10}\text{Be}$ reaction has been

measured for neutron energy higher than 1 MeV, this is the reason why the simulation stops before the end of the ${}^9\text{Be}(\text{d},\text{p}_0){}^{10}\text{Be}$ peak. Apart from the simulated peaks, the peaks of the ${}^9\text{Be}(\text{d},\text{t}){}^8\text{Be}$, ${}^{16}\text{O}(\text{d},\text{p}_0){}^{17}\text{O}$, ${}^2\text{H}(\text{d},\text{p}){}^3\text{H}$, ${}^{16}\text{O}(\text{d},\text{p}_1){}^{17}\text{O}$ and ${}^9\text{Be}(\text{d},\text{a}_0){}^7\text{Li}$ reactions are also observed. These peaks indicate that O and D have also been deposited on the surface of the sample.

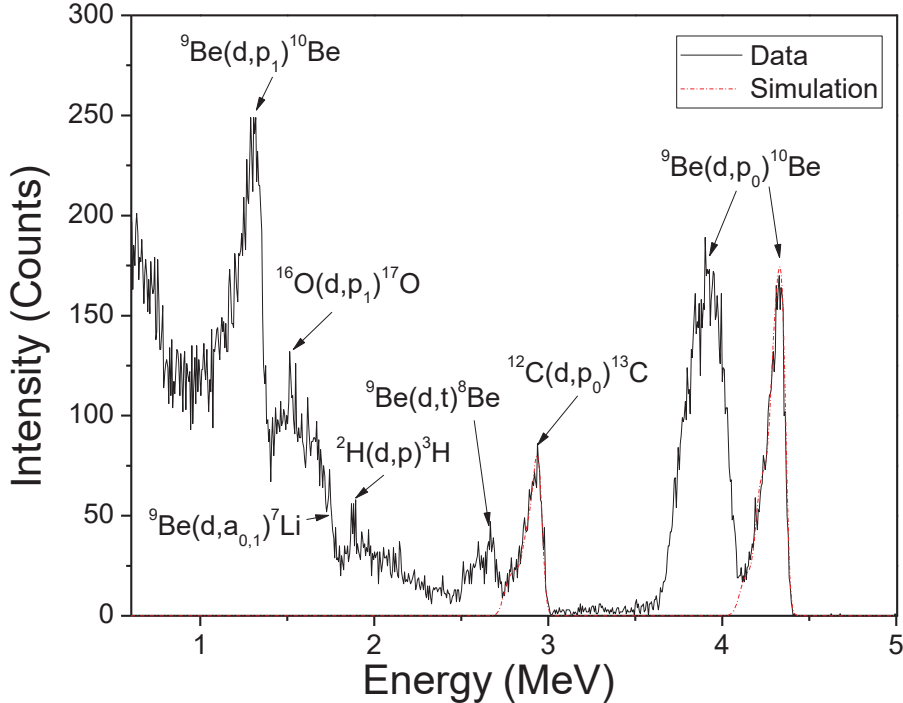


Fig. 2: The NRA experimental (solid line) and simulated (dash line) spectrum of the OPL (120)

From the simulation of the NRA spectra, we can assess the C total surface atomic density and the corresponding deposition depth (Table 1) as well as the C concentration as a function of depth (Fig. 3).

Table 1: Origin of the samples; NRA results for the C total surface atomic density and deposition thickness

Tokamak Area	Tile Area	Campaign Name	Sample Name	C Surface At. Density (10^{17} at/cm^2)	Deposition Thickness (μm)
Dump Plate	Centre (1)	ILW-1	DP (80)	11.8 ± 0.6	6.7
Outer Poloidal Limiter	RH Outer (2)	ILW-1	OPL (120)	2.9 ± 0.2	3
	RH Outer (2)	ILW-2	OPL (320)	0.35 ± 0.07	0.4
Inner Wall Guard Limiter	Centre (3)	ILW-1	IWGL (174)	0.70 ± 0.05	0.8
	RH Outer (4)	ILW-1	IWGL (27)	3.6 ± 0.3	2.3
	RH Outer (4)	ILW-2	IWGL (191)	4.0 ± 0.3	3.7
	RH Wing (5)	ILW-1	IWGL (76)	7.6 ± 0.3	5.5

According to Table 1, DP (80) presents the highest C surface atomic density ($(11.8 \pm 0.6) \times 10^{17} \text{ at/cm}^2$) and deposition thickness (6.7 μm). For the OPL, the sample from ILW-1 campaign (OPL (120)) has more C surface atomic density ($(2.9 \pm 0.2) \times 10^{17} \text{ at/cm}^2$) than from the ILW-2 campaign (OPL (320) ($(0.35 \pm 0.07) \times 10^{17} \text{ at/cm}^2$)). For the IWGL RH Outer, the C surface atomic density does not present significant change from the first (IWGL (27), $(3.6 \pm 0.3) \times 10^{17} \text{ at/cm}^2$) to the second (IWGL (191), $(4.0 \pm 0.3) \times 10^{17} \text{ at/cm}^2$) campaign; for the Centre (IWGL (174)), the C surface atomic density and deposition thickness are quite small ($(0.70 \pm 0.05) \times 10^{17} \text{ at/cm}^2$ and 0.8 μm), while for the RH wing they are quite high ($(7.6 \pm 0.3) \times 10^{17} \text{ at/cm}^2$ and 5.5 μm).

According to Fig. 3, the C concentration has the highest value in the first layer up to 1 μm depth and then it reduces abruptly for all samples except for IWGL (191).

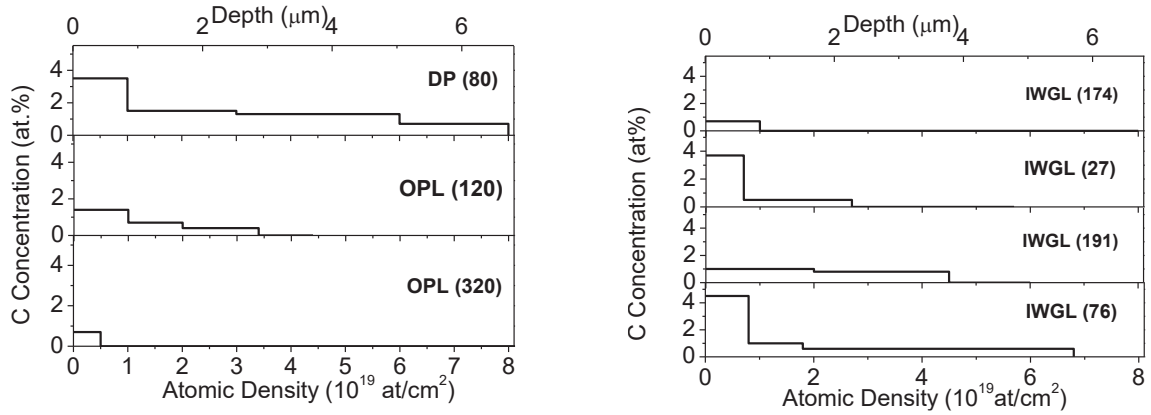


Fig. 3: C depth profile for different areas of the JET tokamak marker tiles

Fig. 4 shows the ${}^9\text{Be}(\text{d},\text{p}_0){}^{10}\text{Be}$ peak of the plasma exposed samples and the reference one. In the reference sample, the peak between the 4 and 4.5 MeV energy corresponds to the Be top layer ($(7.6 \pm 0.1) \mu\text{m}$), the absence of he peak in the region from 3.75 to 4 MeV is related with Ni interlayer and additionally a part of the bulk Be is also detected ($E < 3.75 \text{ MeV}$). The spectra of the sample DP (80) and IWGL (76) shows that after the Be top layer, a mixed layer with Be and Ni has been formed. In samples OPL (120) and IWGL (174), the Be top layer became thinner as a result of the slight erosion ($< 8 \mu\text{m}$) that these samples have been suffered. On the other hand, the Be top layer and Ni interlayer of samples IWGL (320) and IWGL (174) are totally absent, which is probably due to strong erosion ($> 11 \mu\text{m}$). Finally, the sample IWGL (27) has a top layer with low Be concentration which means that a mixed layer has been formed. Probably part of Ni interlayer has come to the surface due to erosion ($8-11 \mu\text{m}$).

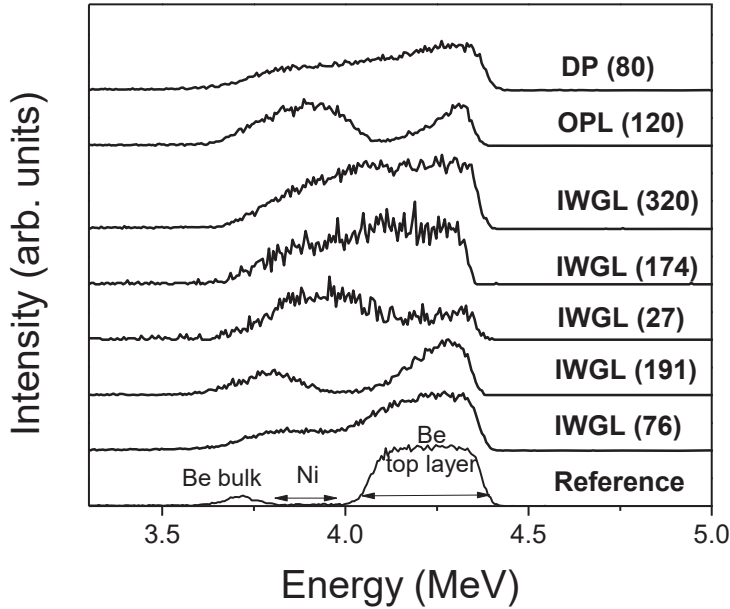


Fig. 4: Comparison of the ${}^9\text{Be}(\text{d},\text{p}_0){}^{10}\text{Be}$ peak between the reference sample and samples after the plasma exposure

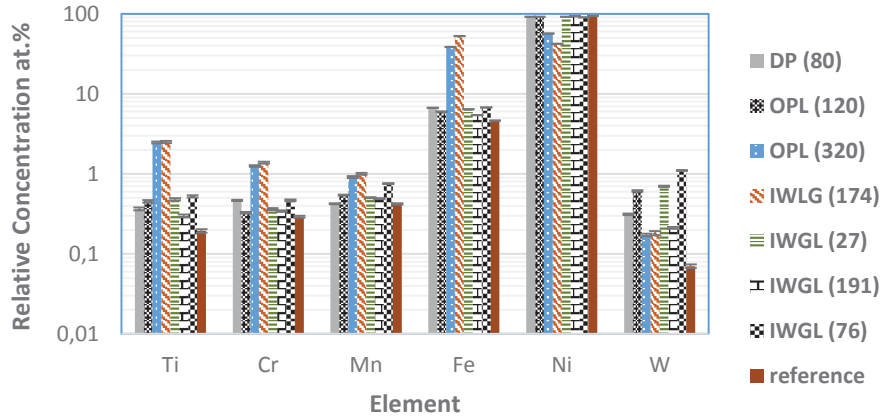


Fig.5: XRF results for exposed to plasma and reference samples

Fig. 5 presents the results of the XRF analysis. This technique detects elements with $Z > 11$, so the elements D, Be, C and O are not detected. In all samples including the reference one, the elements Ti, Cr, Mn, Fe, Ni and W are detected. In samples OPL (320) and IWGL (174), the Ni concentration is much lower than in the reference one; this fact confirms the enhanced erosion of these samples. The W concentration in all samples is much higher than in the reference one, which means that W has been deposited on the main wall tiles during the plasma operation.

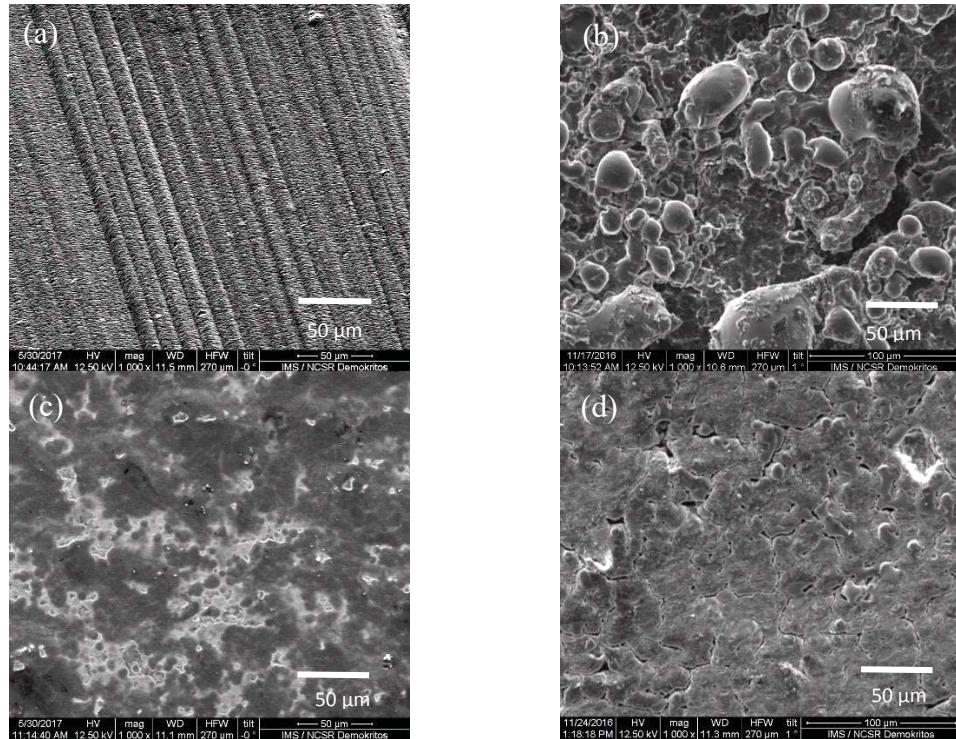


Fig. 6: Images from the SEM analysis with secondary electron of (a) reference sample, (b) DP (80), (c) OPL (120) and (d) IWGL (76)

Fig. 6 shows indicative SEM images of the surface morphology of reference sample and DP (80), OPL (120) and IWGL (76). The DP (80) presents areas with intensive deposition (Fig. 6b). The OPL (120) has some areas rich in Be (dark) and others rich in Ni (light) (fig. 6c), which is interpreted as partial erosion ($< 11 \mu\text{m}$). OPL (320) (not shown) have suffered enhanced erosion ($> 11 \mu\text{m}$) in agreement with the other techniques (NRA and XRF). Prolonged Be structures are observed in sample IWGL (174) (not shown) which has been eroded for depth larger than $11 \mu\text{m}$ (Fig.4). IWGL

(27) presents some areas rich in Be others rich in Ni (not shown) which confirms the partial erosion of the Ni. IWGL (76) seems to have undergone melting (Fig. 6d).

4. Conclusion

Samples retrieved from different Be marker tiles of the JET tokamak main chamber were analysed using various analytical techniques (NRA, XRF and SEM) in order to assess the deposition – erosion and the morphology of the surface. Results of the quantification of C deposition shows that the C surface atomic density varies between $(0.35\pm0.07)\times10^{17}$ and $(11.8\pm0.6)\times10^{17}$ at/cm² while the deposition depth varies between 0.4 and 6.7 μm . Additionally, in all samples except IWGL (191) the C concentration is higher on the surface ($<1\ \mu\text{m}$) than in deeper layers.

The Dump Plate centre area from the ILW-1 campaign presents areas with deposition and the highest C surface atomic density. For the OPL RH outer area samples were investigated from the ILW-1 and ILW-2 campaigns: The sample from the first campaign presents a partial erosion ($<11\ \mu\text{m}$), while from the second the sample has suffered enhanced erosion ($>11\ \mu\text{m}$); additionally the C deposition for the ILW-2 is lower. The IWGL centre area from the ILW-1 campaign suffered strong erosion ($>11\ \mu\text{m}$) and very low C deposition is detected. Regarding the IWGL RH outer area, the sample from ILW-1 campaign has suffered more erosion (the Be top layer is absent) than that from the ILW-2 campaign ($<11\ \mu\text{m}$). Finally the IWGL RH wing presents melting surface and high C deposition.

Acknowledgments

This work was carried out within the EUROfusion Consortium and received funding from the EURATOM research and training programme 2014-2018 under grant agreement number No 633053. The views and opinions expressed herein do not necessarily reflect those of the European Commission.

References

- [1] <https://www.euro-fusion.org/jet/>
- [2] Matthews G F et al 2011 *Phys. Scr.* **T145** .014001 (6pp)
- [3] Rubel M et al 2013 *J. Nucl. Mater.* **438** S1204-S1207
- [4] Lungu C P et al 2007 *Phys. Scr.* **T128** 157-161
- [5] Gurbich A F 2016 *J. Nucl. Intr. Meth. B* **371** 27-32
- [6] Mayer M 1999 *AIP Conf. Proc.* **475** 541-544
- [7] <http://amptek.com/products/complete-xrf-experimenters-kit/>
- [8] NIST SRM 160b, https://www-s.nist.gov/srmors/view_cert.cfm?srm=160B